Beam-blocker-based approaches to cone-beam CT imaging

Seungryong Cho
Department of Nuclear and Quantum Engineering
KAIST
Daejeon, Korea
scho@kaist.ac.kr

***Abstract*—Reduction of radiation dose and correction of scatter in cone-beam CT are important technical issues that need to be addressed when devising a system or applying to clinical applications. In this paper, we show that both scatter correction and dose reduction can be successfully achieved by use of a beam-blocker that is composed of radio-opaque multiple strips. Measurement-based scatter correction method is implemented. Analytic image reconstruction has been developed to reconstruct images when at least half of the cone-beam data are available. Compressive-sensing-inspired iterative algorithm is used to reconstruct images from sparsely sampled data for aggressive dose reduction.**

Keywords—low-dose CT; scatter correction; beam-blocker; image reconstruction

I. INTRODUCTION

Various scatter correction strategies have been introduced, and a good summary can be found in the literature. Beam-blocker-based methods are simple and efficient in terms of hardware implementation, and can achieve scatter estimation without a prior knowledge of the target object. Nonzero signals behind the beam-blockers are attributed to the scatter signals, where the primary beams are assumed to be blocked by the radio-opaque materials such as lead. The scatter components in the open regions can therefore be estimated from the measured scatter in the blocked regions using the interpolation techniques; the interpolation-based estimation is in general legitimate since the scatter distribution is dominantly of low-frequency components. In section II, we demonstrate the scatter correction method and analytic image reconstruction from the partial data where at least half of the cone-beam data are available through the slit openings of the beam-blocker. For more aggressive dose reduction, the area ratio of the openings over the entire field-of-view is reduced down to 25% and iterative image reconstruction has been performed from such sparsely sampled data as will be discussed in section III.

II. SCATTER CORRECTION AND ANALYTIC RECONSTRUCTION

A. Scatter correction

The scatter dominantly carries low-frequency component and is rather insensitive to small deformations of the internal anatomy. Accordingly, the scatter distribution can be estimated from the partially blocked projection data using an interpolation method. We estimated the scatter in the following processes. First, the raw projection data were filtered by a moving average filter in horizontal direction to reduce unwanted high-frequency noise in the scatter estimation. The moving average filter generates a smoothing effect by taking average value of the selected interval. We used only the central portion of the shadow for scatter estimation; therefore, the discontinuity due to the beam-blocker did not complicate the scatter estimation process. Second, we estimated the scatter from the data under the blocked region by use of a 1D piecewise cubic interpolation. Third, we applied a weighting function to restrict the scatter correction area within the object support which has slightly extended boundaries than the true object's.

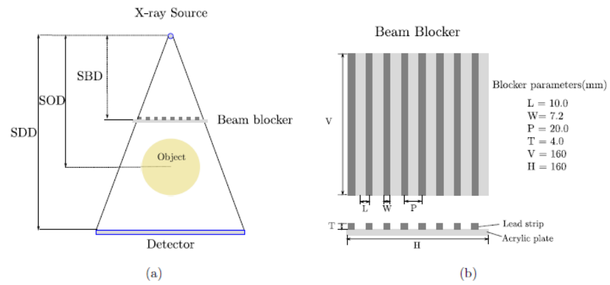

Figure 1. Schematic of beam-blocker-based scanning geometry.

B. Analytic image reconstruction

We developed a rebinned backprojection-filtration (BPF) algorithm for reconstructing images from the partially blocked cone-beam data. Since we placed the beam-blocker so that the strips are aligned parallel to the rotation axis direction, the partial data thus acquired would yield discontinuities along the fan-direction. Due to the discontinuities in the projection data, conventional FBP-type algorithms cannot be directly applied to image reconstruction. In contrast, the BPF algorithm performs the filtering process in the last step in the image domain, and therefore reconstruction is more robust against discontinuous data than the FBP algorithm. We utilized the data redundancy in the mid-plane fan beam data and quasi-redundancy in the off-midplanes in cone-beam data by designing the beam-blocker so that one can achieve enough data for image reconstruction. The fan-to-parallel rebinning process removes the spatially dependent weighting factor in the backprojection step, which helps avoiding the ring artifacts that are associated with the partial beam weighting. The reconstructed images are shown in Fig. 2 with scatter-contaminated image for comparison.

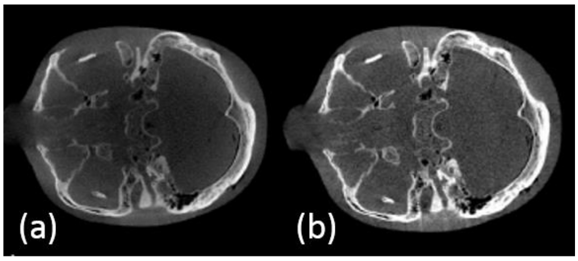

Figure 2. (a) Scatter-contaminated image, (b) scatter-corrected image.

III. Dose reduction and iterative reconstruction

As an alternative approach of sparse-view sampling, researchers including us have earlier proposed a sparse sampling technique that uses a moving beam-blocker and have experimentally demonstrated its feasibility in CBCT applications. In the beam-blocker-based approach, the x-ray cone-beam is partially blocked by multiple radio-opaque strips that are placed between the x-ray source and the patient. To increase sampling uniformity and data incoherence, we implemented a reciprocating motion of the beam-blocker in either sinusoidal motion or linear motion. The radio-opaque strips can be aligned either parallel to or perpendicular to the longitudinal direction (rotation axis) of the scanner, and the related reciprocating motion can be aligned perpendicularly or in parallel to the longitudinal axis, respectively. As has been shown in our earlier work, the latter case would lead to a bunched sparse-view data and the resulting reconstructed image quality would turn out to be inferior. Therefore, we have focused on the sparse sampling scheme that uses a scanning scheme as shown in Fig. 3. The reconstructed images are shown in Fig. 4 and more details on the image reconstruction process will be discussed in the conference.

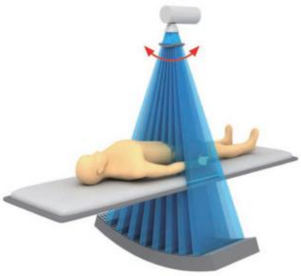

Figure 3. Schematic of moving beam-blocker-based sparse sampling scan.

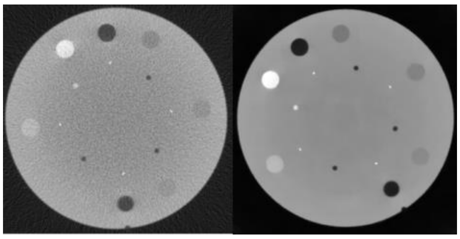

Figure 4. Reconstructed image from low-tube current (left) vs from sparsely sampled data (right).

IV. Discussion

In this work, the beam-blocker-based scatter correction and sparse sampling approach as an alternative of sparse-view sampling for low-dose CT has been applied to a CBCT scanner. A successful image reconstruction has been demonstrated from the sparsely sampled data according to the proposed method, and successful scatter correction has been achieved. With further optimizations, we envision that the proposed approach can be effectively used for low-dose scatter-free CBCT.

References

[1] J. Min, R. Pua, I. Kim, B. Han, and S. Cho, "Analytic image reconstruction from partial data for a single-scan cone-beam CT with scatter correction," Med. Phys., vol. 42, pp. 6625-6640, 2015.

[2] S. Cho, T. Lee, J. Min, and H. Chung, "Feasibility study on many-view under-sampling technique for low-dose computed tomography," Opt. Eng., vol. 51, pp. 080501 (4pp), 2012.

[3] J. Wang, W. Mao, and T. Solberg, "Scatter correction for cone-beam computed tomography using one-dimensional moving blocker strips: a preliminary study", Med. Phys. vol. 37 pp. 5792-800, 2010.

[4] S. Abbas, T. Lee, S. Shin, R. Lee, and S. Cho, "Effects of sparse sampling schemes on image quality in low-dose CT," Med. Phys., vol. 40, pp. 111915 (12pp), 2013.

[5] T. Lee, C. Lee, J. Baek, and S. Cho, "Optimization of MVUS in cone-beam CT," (in review), 2015.

Automated selection of major artery-vein pairs for measurement of arteriolar-to-venular diameter ratio on retinal images

Yuji Hatanaka, Hirokazu Tachiki,
Susumu Okumura and Kazunori Ogohara
School of Engineering, the University of Shiga Prefecture
Hassaka-cho 2500, Hikone-shi, Shiga 522-8533, Japan
hatanaka.y@usp.ac.jp

Chisako Muramatsu and Hiroshi Fujita
Graduate School of Medicine, Gifu University
Yanagido 1-1, Gifu-shi, Gifu 501-1194, Japan

***Abstract*— For measurement of arteriolar-to-venular diameter ratio, an automated selection of major artery-vein pairs is presented. We proposed such a method, but the accuracy of major arteries and veins was low. The proposed method includes retinal vessel segmentation, major vein extraction, and major artery extraction. The major vein is selected in the red component of the color image, and the major artery is also selected in the green component image. The proposed method and the previous one were evaluated using 22 retinal images with 44 artery-vein pairs. The accuracies of major veins was changed 80% to 98%. The accuracy of the major arteries was also changed 71% to 77%. The proposed method may be useful for measurement of arteriolar-to-venular diameter ratio.**

Keywords*— *selection of major artery-vein pairs, hypertensive retinopathy, random forest, absorptivity, computer-aided detection

I. INTRODUCTION

The number of patients with hypertension is currently one per three people in Japan. Retinas permit noninvasive observation of the retinal vasculature, which can indicate health conditions, such as diabetes and hypertension. One of the hypertension-associated findings in retinal images is arteriolar narrowing, which can be assessed by arteriolar-to-venular diameter ratios (AVR). Ophthalmologists rely on retinal images during medical check-up or mass screenings. However, they observe the condition of blood vessels by eye measurement, so this method is not quantitative measurement. Therefore, several research groups have made efforts in developing automated AVR measurement [1-3]. Niemeijer et al. [1] proposed an automated selection of major artery-vein pairs. The pairs were matched using an iterative algorithm with the features on the centerline pixel of the blood vessels. We also proposed a method using a linear discriminant classifier with eight features on the centerline of the blood vessels [2, 3]. But, their methods were strong depended to accuracy of the centerline extraction. In this study, artery-vein pair selection is improved based on the vein extraction in the red component of color image.

II. METHODS

The proposed method consists of the following 3 steps: blood vessel segmentation, major vein extraction, and major artery extraction. The blood vessels were first segmented by using black-top-hat transformation combined with double-ring filter technique in the green component of color images. An artery is hardly seen in the red component of color image so that an arterial blood includes lots oxyhemoglobin, which absorptivity is low in the red wavelength. Therefore, the veins are selected by using the linear discriminant function with 8 features [3] in the red component of color images. The thick vein candidate is also selected as the major vein by measurement of vein diameter. Moreover, the artery candidates are extracted by elimination of the vein candidates from the blood vessel candidates in the green channel of the color images. The major artery is finally selected by decision tree using three features, which are artery candidate diameter, candidate area, and angle difference between the candidate and the major vein nearest to it.

III. RESULTS AND CONCLUSION

The proposed method was evaluated by using cross validation in twenty two retinal images. As a result, 100% of the major veins were detected when 77% of the major arteries were detected. When our previous method was evaluated in same images, the detection rates of the veins and arteries were 80% and 71%, respectively [3]. Thus, although it is evident that the proposed method can detect veins, arteries detection must be considered. We also have been improving a blood vessel detection, thus it will be applied to the proposed method in the future.

REFERENCES

[1] M. Niemeijer, X. Xu, A.V. Dumitrescu, et al., “Automated measurement of the arteriolar-to-venular width ratio in digital color fundus photographs,” IEEE Trans. Med. Img., vol.30, no.11, pp.501–509, Nov. 2011.

[2] C. Muramatsu, Y. Hatanaka, T. Iwase, et al., “Automated selection of major arteries and veins for measurement of arteriolar-to-venular diameter ratio on retinal fundus images,” Comput. Med. Imag. Graph., vol. 35, pp.472–480, Sep. 2011.

[3] C. Muramatsu, A. Mizukami, Y. Hatanaka, et al., “Improvement on recognition of major arteries and veins on retinal fundus images by template matching with vessel models,” Med. Img. Info. Sci., vol. 30, no. 3, pp. 63-69, 2013.

Analytical Metal Artiact Corrector for Polychromatic X-ray CT

Hyoung Suk Park
Department of Computational Science and Engineering
Yonsei University, Seoul, 120-749, South Korea
jiro7733@yonsei.ac.kr

***Abstract*—X-ray computed tomography (X-ray CT) is the most widely used tomographic imaging technique in the field of dental and medical radiography. In spite of the excellent resolution and contrast of the cross-sectional images, its advantage is partly limited by the metallic object-related artifacts in the images. Metal artifacts are mainly caused by the beam-hardening of polychromatic X-ray photon beams, which causes mismatch between the actual sinogram data (or X-ray data) and the data model being the Radon transform of the unknown attenuation distribution in the CT reconstruction algorithm. In this presentation, we introduce a new method to correct metal artifacts for polychromatic X-ray computed tomography without degrading intact anatomical images. Without prior knowledge of the spectrum parameters or energy-dependent attenuation coefficients, the proposed correction allows the background CT image (i.e., the image before its corruption by beam-hardening artifacts) to be extracted from the uncorrected CT image. Numerical simulations and experiment demonstrate the effectiveness of the proposed method to alleviate metal artifacts due to beam hardening.**

Keywords—computed tomography, beam hardening, metal artifacts, Radon transform

I. INTRODUCTION

This paper focuses on reducing metal artifacts due to beam hardening effect in computerized tomography (CT), generated by medical implants including orthopedic implants, dental fillings, surgical clips, and coronary stents. The presence of metallic objects in the scan field is known to generate severe discrepancy between the projection data (P) and the Radon transform ($\mathrm{Rf}_{\mathrm{E}_0}$). This severe mismatch causes the bright and dark streaking or cupping artifacts in CT image generated by conventional reconstruction algorithm, called filtered backprojection (FBP) [1].

In [2], we have proposed a metal artifacts correction method that makes use of shape information of metallic implants to correct the mismatch of P-$\mathrm{Rf}_{\mathrm{E}_0}$ in FBP. This metal artifact corrector makes it possible to reveal background CT image corrupted by metal artifacts from CT image. Numerical simulation shows the validity of the artifacts correction method.

II. METHOD

Considering 2-dimensional parallel beam system, the projection data is given by Lambert-Beer's law [3,4]:

$$\mathrm{P}(\varphi, \mathrm{s}) = -\ln \int \eta\,(E) \exp\{-\mathrm{Rf}_{\mathrm{E}}(\varphi, \mathrm{s})\}\,\mathrm{dE},$$

where $\mathrm{f}_{\mathrm{E}}(\mathrm{x})$ denotes the attenuation coefficient at position x and energy E, $\eta(\mathrm{E})$ represents normalized x-ray spectrum as a function of energy E. The standard CT reconstruction method is the filtered backprojection (FBP) given by

$$\mathrm{f}_{\mathrm{CT}}(\mathrm{x}) \coloneqq R^{-1}P(\mathrm{x})$$

Here, R^{-1} denotes the FBP operator.

Assume that $\mathrm{f}_{\mathrm{E}_0}$ is an unknown target image to be reconstructed and D is the domain occupying the metal regions. Following the paper [2], the CT image can be corrected by the following relation:

$$\mathrm{f}_{\mathrm{CT}}(\mathrm{x}) - \phi_{\mathrm{D},\lambda}(\mathrm{x}) = \mathrm{f}_{\mathrm{E}_0}(\mathrm{x}),$$

where $\phi_{\mathrm{D},\lambda}$ denotes the analytical metal artifact corrector corresponding to mismatch of P-$\mathrm{Rf}_{\mathrm{E}_0}$, which is given by

$$\phi_{\mathrm{D},\lambda}(\mathrm{x}) = -R^{-1}\left[ln\left(\frac{\sinh(\lambda R_{\chi_D})}{\lambda R_{\chi_D}}\right)\right](\mathrm{x}).$$

Here, λ is parameter depending on the incident X-ray spectrum and attenuation coefficient of objects to be imaged.

A. Artifacts Correction Algorithm

The proposed metal artifacts correction algorithm simply consists of the following two steps.
1. Segment the metal region D in f_{CT}.
2. Determine the parameter λ minimizing the following problem:

$$\mathrm{argmin}_{\lambda} \int_{R^2/D} |\nabla(\mathrm{f}_{\mathrm{CT}}(\mathrm{x}) - \phi_{\mathrm{D},\lambda}(\mathrm{x})|^2\,\mathrm{dx}$$

The parameter λ is chosen in such a way that $\phi_{\mathrm{D},\lambda}$ reduces the streaking artifacts in CT image.

III. RESULTS

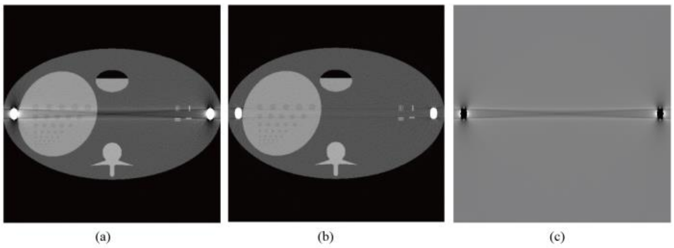

Fig. 1 Numerical simulation for abdomen phantom containing two metallic objects. (a) CT image (f_{CT}) (b) corrected image ($f_{CT} - \phi_{D,\lambda}$) (c) beam hardening corrector $\phi_{D,\lambda}$

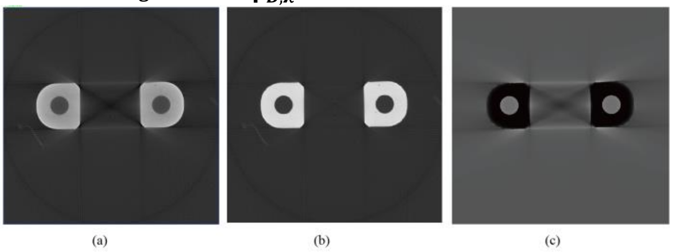

Fig. 2 Experimental result for two metallic objects. (a) CT image (f_{CT}) (b) corrected image ($f_{CT} - \phi_{D,\lambda}$) (c) beam hardening corrector $\phi_{D,\lambda}$

Fig. 1 and 2 shows the numerical simulation and experiment for metal artifact correction method, respectively. As can be seen, metal streaking artifacts are significantly reduced in the corrected image ($f_{CT} - \phi_{D,\lambda}$).

IV. CONCLUSION

With the presence of metallic objects in the field of view of CT, the reconstructed image f_{CT} suffer from severe streaking artifacts and they lead to degradation of quality of CT image. We introduce the metal artifact correction method based on the metal artifact corrector $\phi_{D,\lambda}$. By subtracting $\phi_{D,\lambda}$ from f_{CT}, streaking artifacts are removed or alleviated, and details near the metallic objects become much more visible.

ACKNOWLEDGMENT

This work was supported by Samsung Science & Technology Foundation (No. SSTF-BA1402-01).

REFERENCES

[1] R. N. Bracewell, and A. C. Riddle, “Inversion of fan-beam scans in radio astronomy,” The Astrophysical Journal, vol. 150, pp. 427, 1967.

[2] H. S. Park, D. Hwang, and J. K. Seo, “Metal Artifact Reduction for Polychromatic X-ray CT Based on a Beam-hardening Corrector”, IEEE transactions on medical imaging, in press.

[3] A. Beer, “Bestimmung der absorption des rothen lichts in farbigen flussigkeiten”, Annalen der Physik, Vol 162, pp. 78–88, 1852.

[4] J. H. Lambert and E. Anding, “Lamberts Photometrie: Photometria, sive De mensura et gradibus luminis, colorum et umbrae”, Ostwalds Klassiker der exakten Wissenschaften, Vol. 1-2, 1892.

Composite recognition of the iliopsoas muscle based on the muscle direction modeling in CT images*

Naoki KAMIYA
School of Information Science and Technology
Aichi Prefectural University
Nagakute, Aichi, JAPAN
n-kamiya@ist.aichi-pu.ac.jp

Xiangrong ZHOU, Chisako MURAMATSU, Takeshi HARA and Hiroshi FUJITA
Department of Intelligent Image Information
Graduate School of Medicine, Gifu University
Gifu, Gifu, JAPAN

Hiroki KATO
Department of Radiology
Gifu University School of Medicine
Gifu, Gifu, JAPAN

Huayue CHEN
Department of Anatomy, School of Medicine
University of Occupational and Environmental Health
Kitakyushu, Fukuoka, JAPAN

***Abstract*—Iliopsoas muscle is one of the important skeletal muscle related to ambulatory function. Iliopsoas muscle consists of psoas major and iliac muscles. Quantitative analysis of the iliopsoas is considered to lead to support of fall arrest in the elderly. In this paper, we propose an automatic recognition method of the iliopsoas muscle based on the muscle direction modeling in CT images. We have developed site-specific recognition method of skeletal muscle in torso region using CT images without contrast. The implementation of quantitative analysis of the iliopsoas muscle is required composite recognition of psoas major and iliac muscle which is part of the iliopsoas. We describe the modeling method of a muscle fiber direction of iliopsoas muscle and the recognition method of the iliopsoas muscle. Muscle fibers of the iliopsoas muscle has a characteristic running. In this paper, the modeling technique of the muscle direction was described. In recognition, applying the muscle fiber model on the anatomical feature points (LMs), to detect the each muscle position for allocate shape model. The recognition result in five cases, obtained 73.2 % average concordance rate. In visual evaluation in 20 cases, over extraction is not to other organs at 85% of cases, we got good results. The proposed method is considered to be effective in the recognition of the initial region of the iliopsoas muscle. In the future, development of a sophisticated muscle function analysis method is necessary.**

Keywords—iliopsoas muscle; muscle direction model; psoas major muscle; iliac muscle

I. Introduction

Iliopsoas muscle is one of the important skeletal muscle related to ambulatory function. The muscles related to ambulatory function has psoas major muscle and iliac muscle, and defined as iliopsoas muscle. We have proposed an automatic recognition method of the iliopsoas muscle. Iliopsoas muscle to the subject of this study, is strongly associated with the failure by the fall of the elderly. The elderly of fall is due to functional deterioration of the iliopsoas muscle consisting of the psoas major and the iliac muscle [1]. Further, including the iliopsoas muscle, skeletal muscle decreases with age. Therefore, quantitative analysis of the iliopsoas is considered to lead to support of fall arrest in the elderly.

We have developed site-specific recognition method of skeletal muscle using torso CT images without contrast [2]. In particular, automatic recognition method of psoas major muscle closely related with the iliopsoas muscle has already been established [3]. Similarly, we also proposed the recognition method of the iliac muscle as initial study [4]. Therefore, the implementation of quantitative analysis of the iliopsoas muscle associated with walking ability is required composite recognition of psoas major muscle and iliac muscle which is part of the iliopsoas.

In this study, we propose a modeling method of the muscle fibers of the psoas major and iliac muscle with the characteristic running, and also propose a method to use the model for recognition of these muscles. By the recognition of theses muscles, quantitative analysis of these area, volume and shape can be realized in the iliopsoas region.

II. Methods

We describe the modeling method of a muscle fiber direction of iliopsoas muscle and the recognition method of the iliopsoas muscle using this model in torso CT images. Figure 1 shows the schematic view of our proposed method. The input images are torso CT image without contrast and skeletal images. The skeletal images are generated by classifying the recognized bone region using the gray value form the torso CT images automatically [5].

A. Muscle Direction Modeling and Featurepoint Detection

Muscle fibers of the iliac muscle has a characteristic running. Therefore, using a 20 cases of training database, and

This research was supported in part by a Grant-in-Aid for Scientific Research on Innovative Areas, MEXT. and Grant-in-Aid for Young Scientists (B), JSPS, Japanese Government.

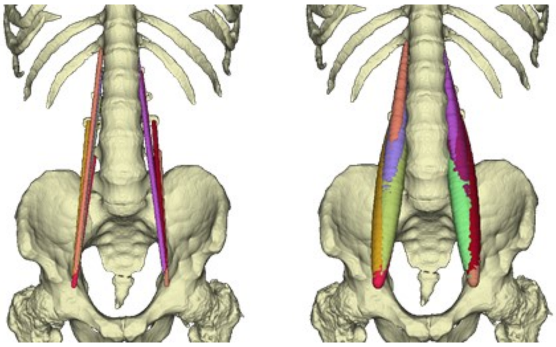

(a) Psoas major muscle

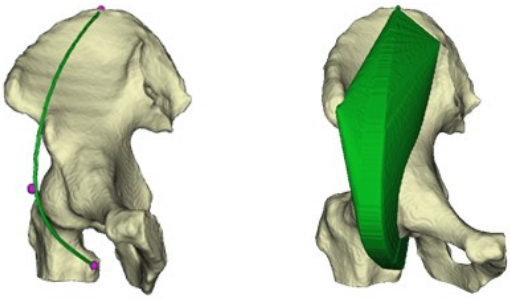

(b) Iliac muscle (Right side)

Fig. 1. Muscle direction model of psoas major and iliac muscle
(Left: Muscle fiber, Right: Shape model)

to model the curvature and length of the muscle fibers of the iliac muscles. On the other hand, muscle fibers of the psoas major muscle, the muscle fiber is approximated by connecting anatomical feature point by a straight line. Next, as an anatomical position feature of these muscle, landmarks (Landmarks: LMs) corresponding to the origin and insertion are recognized on the skeletal image.

B. Recognition

In recognition, estimate the existing position of the iliac muscle by applying the muscle fiber model. Specifically, to generate an approximation mask using a muscle fiber model, to obtain a candidate region of the iliac muscle. Finally, recognize the muscle region using gray value and edge information.

III. Experiment and Results

By using 20 cases of the torso CT images without contrast and no abnormality in the muscle region. The image that was created under the guidance of a physician to obtain a gold standard image. The average concordance rate in this evaluation experiment referred to the Jaccard similarity coefficient values, recall rate and adaption rate with 5 cases. In addition, visual evaluation was carried out using the 20 cases. The recognition result in five cases, obtained 73.2 % average concordance rate. In visual evaluation, over extraction is not to other organs at 85% of cases, we got good results. Figure 2 shows the 3-D view of the recognition results and comparison with gold standard.

Fig. 2. Comparison of the recognition result with gold standard
(Green: Overlap, Red: Unver extraction, Blue: Over extraction)

This result is due to the fact that the running of the muscle fibers of the iliac muscle has been correctly modeling. In particular, the running curve of the muscle fiber can be satisfactory expressed, it is considered that a summary of individual differences can be realized.

IV. Conclusion

In this study, automated recognition of the iliopsoas muscle and modeling of the muscle direction was achieved. The running pattern of the muscle fibers of the iliac and psoas major muscles was depicted, and modeling of the characteristic curve that connects the origin, insertion, and initial areas of the iliopsoas was achieved. Therefore, it was possible to satisfactorily recognize region of iliopsoas muscle. To verify the validity of the method using a number of experimental cases is a future work. Furthermore, it is necessary to sophisticated to muscle function analysis.

References

[1] K. Takahashi, H. Nakadaira, and M. amamoto, "Different changes of quantity due to aging in the psoas major and quadriceps femoris muscles in women,"Niigata Journal of Health and Welfare (in Japanese), vol.6, no.1, pp.16-21, 2006.

[2] N. Kamiya, "Fully automatic recognition of the skeletal muscles in non-contrast torso CT images: Present and future prospectives," Journal of Medical Imaging and Information Sciences (in Japanese), vol.31, no.2, pp.xxxii-xxxv, 2014.

[3] N. Kamiya, X. Zhou, H. Chen, C. Muramatsu, T. Hara, R. Yokoyama, M. Kanematsu, H. Hoshi, and H. Fujita, "Automated segmentation of psoas major muscle in X-ray CT images by use of a shape model: Preliminary study, " Radiological Physics and Technology, vol.5, no.1, pp.5-14, 2012.

[4] H. Fujita, T. Hara, X. Zhou, C. Muramatsu, N. Kamiya, M. Zhang, D. Fukuoka, Y. Hatanaka, T. Matsubara, A. Teramoto, Y. Uchiyama, H. Chen and H. Hoshi, "Model Construction for Computational Anatomy: Progress Overview FY2009-FY2013", Proceedings of the Fifth International Symposium on the Project "Computational Anatomy", pp.25-35, 2014.

[5] X. Zhou, T. Hayashi, M. Han, H. Chen, T. Hara, H. Fujita, R. Yokoyama, M. Kanematsu, and H. Hoshi, "Automated segmentation and recognition of the bone structure in non- contrast torso CT images using implicit anatomical knowledge, " Proc. SPIE, 7259, 72593S. doi:10.1117/12.812945,2009.

Medical-Image-based computer- and robot-assisted surgery

:Experience at Asan Medical Center, South Korea

Kim, Namkug
Dept. of Convergence Medicine/Radiology
Asan Medical Center, Univ. of Ulsan College of Medicine
Seoul, South Korea
namkugkim@gmail.com

***Abstract*—Nowadays, most of medical images can be digitalized and used for various clinical purposes. However, the usability of archived images is far from satisfaction. In the field of medicine, the images are referred only once by a radiologist and clinician for diagnosis and treatment and then discarded into the repository. However, the rapid development of recent medical imaging modality which produces a very accurate image data could be used for additional computer aided surgical procedure. This situation made me interested in medical imaging processing and surgery supports including image guided navigator/surgery system. In this talk, various medical-image-based surgery supports including computer assisted surgery and robot assisted surgery of mine will be presented. The basic technology of them includes medical image processing, image segmentation, registration, image analysis, surgery planning, surgical navigator, 3D printer, etc. My experience of working with various kinds of radiologists and surgeons including oral and orthopedic, plastic, maxilla-facial surgery and orthodontics of Seoul National University, University of Ulsan College of Medicine, etc will be presented also. Based on these experiences, I'll cover various topics related with computer- and robot-assisted surgery.**

Keywords— medical images; computer-aissisted surgery; robot-assisted surgery

[1] Perfusion- and Pattern-based Quantitative CT Indexes Using Contrast-Enhanced Dual-Energy Computed Tomography in Diffuse Interstitial Lung Disease: Relationships with Physiologic Impairment and Prediction of Prognosis, Jung Won Moon; Jang Pyo Bae; Ho Yun Lee; Namkug Kim*; Man Pyo Chung; Hye Yun Park; Yongjun Chang; Joon Beom Seo; Kyung Soo Lee, Eur Radiol. 2015 Aug 9. [Epub ahead of print], 26253261 (co_CA)

[2] Automatic Left and Right Lung Separation Using Free-formed Surface Fitting on Volumetric CT, Youn Joo Lee1, Minho Lee, Namkug Kim*, Joon Beom Seo2, Joo Young Park2, Journal of digital imaging(1.421), August 2014, Volume 27, Issue 4, pp 538-547I.S. Jacobs and C.P. Bean, “Fine particles, thin films and exchange anisotropy,” in Magnetism, vol. III, G.T. Rado and H. Suhl, Eds. New York: Academic, 1963, pp. 271-350.

[3] Thoracic cavity segmentation algorithm using multiorgan extraction and surface fitting in volumetric CT, JangPyo Bae, Namkug Kim*, Sang Min Lee, Joon Beom Seo, Hee Chan Lee, Med Phys(3.761), 2014, 41, 041908 (2014) 24694139

[4] Performance enhancement of Respiratory Tumor Motion Prediction Using Adaptive Support Vector Regression: Comparison with Adaptive Neural Network Method. SeungWook Choi1, Yongjun Chang2, Namkug Kim*, Sung Ho Park3, Si Yeol Song3, Heung Sik Kang1, International Journal of Imaging Systems and Technology 24 (1), 8-15

[5] Automatic reconstruction of the arterial and venous trees on volumetric chest CT, Seyoun Park, Sang Min Lee, Namkug Kim*, and Joon Beom Seo, Hayong Shin, Med. Phys(3.761), 2013 Jul;40(7):071906

[6] A Support Vector Machine Classifier Reduces Inter-Scanner Variation in the HRCT Classification of Regional Disease Pattern in Diffuse Lung Disease, Yongjun Chang, Jonghyuck Lim, Namkug Kim*, Joon Beom Seo David A. Lynch, Medical Physics (3.761), 2013 May;40(5):05191

[7] Fast and efficient lung disease classification using hierarchical one-against-all support vector machine and cost-sensitive feature selection. Chang Y, Kim N*, Lee Y, Lim J, Seo JB, Lee YK., Comput Biol Med. (1.127) 2012 Nov 14. pii: S0010-4825(12)00165-5. doi: 10.1016/j.compbiomed.2012.10.001., 23158697

[8] Regional Context-sensitive Support Vector Machine Classifier to Improve Automated Identification of Regional Pattern of Diffuse Interstitial Lung Disease. Lim JH, Kim N*, Seo JB, Lee YK, Lee Y, Kang SH, Journal of Digital Imaging(1.421), 2011 Dec;24(6):1133-40, 21311944

[9] Performance testing of several classifiers for differentiating obstructive lung diseases based on texture analysis at high-resolution computerized tomography (HRCT). Y. Lee, J.B. Seo, J.G. Lee, S.S. Kim, N. Kim*, and S.H. Kang, Comput Meth Prog Bio(1.238), 2009. 93(2): p. 206-15. 19070933

Lung Tumor Tracking during Radiotherapy Treatment using 4D CT Image-based Treatment Planning

Helen Hong*,Julip Jung
Department of Multimedia Engineering
Seoul Women's University
Seoul, Republic of Korea
hlhong, jjulip@swu.ac.kr

Inbum Lee, Sooyeol Lee
Medical Imaging Research Section,
Electronic & Telecommunication Research Institute,
Daejeon, Republic of Korea
iblee@slmed.co.kr, seq@etri.re.kr

Abstract*— The 4D CT image-based treatment planning is used to precisely deliver of radiation dose to moving targets while avoiding surrounding normal tissues in radiotherapy of lung cancer. However, lung tumor motion during treatment can be different due to respiratory motion and cardiac motion. We propose a tumor tracking method that estimate patient-specific tumor motion using consecutive deformable registration in 4D planning CT images and compensate respiratory motion differences between planning and treatment CT images using tumor template matching. For simulation of different tumor motion and respiratory motion between planning CT and treatment CT images, we generated 4D XCAT phantoms with different tumor and respiratory motion. Each phantom was created with 0.75x0.75x1.5mm3 voxel size, 5s respiratory period with ten phases. The sphere-shaped tumor with diameter of 1.6-4.4cm is added at different location of the lung. In planning stage, to estimate patient-specific tumor motion, global tumor motion is estimated by calculating a respiration rate of each phase through the 3D affine registration between end-inspiration(EI) and end-expiration(EE). Then, local tumor motion is estimated by deformable registration between neighbor phases from EI to EE. In treatment stage, to compensate respiratory motion differences between planning and treatment CT images, the patient-specific tumor motion is globally refined by the 3D affine registration between corresponding phase images of planning CT and treatment CT. Then, local tumor motion is corrected by tumor template matching with intensity and geometric similarities. For evaluation of tumor tracking accuracy, tumor localization error of the global motion refinement in treatment stage (A) and the local motion correction in treatment stage (B) was measured by calculating root-mean-squared distance between tumor centroids of ground truth and treatment CT images. Our tumor tracking method can predict tumor location during radiotherapy treatment and simplify the procedure in treatment stage by using patient-specific motion estimated in planning stage.

Keywords—lung tumor tracking, radiotherapy treatment, 4D CT

ACKNOWLEDGMENT

This work was supported by the Korea research council for industrial science and technology program (B551179-12-08-00, Development of Convergent Radio Therapy Equipment with O-arm CT) funded by the Ministry of Knowledge Economy (MKE, Korea).

* Corresponding author. Email. hlhong@swu.ac.kr, Phone. +82 2 970 5756